J Nanopart Res (2012) 14:766
DOI 10.1007/s11051-012-0766-z

RESEARCH PAPER

Nanoscale near-field infrared spectroscopic imaging of silica-shell/gold-core and pure silica nanoparticles

Zachary Nuño · Brandon Hessler · Bryan Heiberg · Ralph Damato · Terry Dunlap · Young-Seok Shon · Yohannes Abate

Received: 26 September 2011 / Accepted: 30 January 2012

Abstract Spectroscopic near-field imaging of single silica-shell/Au-core and pure silica nanoparticles deposited on a silicon substrate is performed in the infrared wavelength range ($\lambda = 9$–11 μm) using scattering-type scanning near-field optical microscopy (s-SNOM). By tuning the wavelength of the incident light, we have acquired information on the spectral phonon–polariton resonant near-field interactions of the silica-shell/Au-core and pure silica nanoparticles with the probing tip. We made use of the enhanced near-field coupling between the high index Au-core and the probing tip to achieve spectral near-field contrast of the thin silica coating (thickness < 10 nm). Our results show that spectroscopic imaging of thin coating layers and complex core–shell nanoparticles can be directly performed by s-SNOM.

Keywords Silica-shell · Scattering-type scanning near-field optical microscopy (s-SNOM) · Coating layers · Core–shell nanoparticles · Near-field infrared imaging

Z. Nuño · B. Hessler · B. Heiberg · R. Damato · T. Dunlap · Y. Abate (✉)
Department of Physics and Astronomy, California State University Long Beach, California, CA 90840, USA
e-mail: yabate2@csulb.edu

Y.-S. Shon
Department of Chemistry and Biochemistry, California State University Long Beach, California, CA 90840, USA

Introduction

Coated nanoparticles and core–shell nanostructures offer modified physical, electrical, and optical properties that are of interest in electronics, photonics, catalysis, nanotechnology, and biomedical research (Bao et al. 2010; Berndt et al. 2006; Lawrie et al. 2003; Teng et al. 2004; Yu et al. 2005; Zimmer et al. 2006). Coated nanoparticles have been used in a wide range of applications from environmental solutions and green chemistry to biology and medicine (Basiruddin et al. 2010). The coating or encapsulation of nanoparticles is of specific interest for the controlled release of drugs, genes, and other bioactive agents (Wang et al. 2004). Coatings of nanoparticles provide the benefits of protection from rapid degradation, targeting delivery, control of the release rate, and prolonged duration of bioactive agents. Coating of semiconductor quantum dots by inorganic semiconducting materials can result in improved quantum confinement efficiency (Zou et al. 1999). Nanoparticle encapsulation technologies produce highly water-soluble and bright quantum dots (QDs) that are capable of protecting QDs from chemical-induced degradation or surface modification (Hu and Gao 2010). Stable coatings could maintain QD integrity and optical properties under complex chemical environments (Hu and Gao 2010). But investigation of the optical properties of thin coating layers on nanoparticle surfaces is difficult due to lack of high spatial optical resolution.

Published online: 14 February 2012

Sub-wavelength optical detection techniques allow direct, fast, nondestructive, and sensitive information of a wide range of nanomaterials characterized by various chemical compositions, refractive index, charge carrier density and crystal structure. Among different sub-wavelength optical detection techniques, scattering-type scanning near-field optical microscopy (s-SNOM) has been demonstrated to achieve images with a spatial resolution less than tens of nanometers independent of the wavelength of light used. s-SNOM has been applied in a wide range of frequencies including visible (Kim and Leone 2006; Ogawa et al. 2010), infrared (Amarie et al. 2009; Cvitkovic et al. 2006), and terahertz (Huber et al. 2008a, b) to investigate the local structural properties (Huber et al. 2006), material composition (Hillenbrand and Keilmann 2002), plasmonic modes (Kim et al. 2009; Schnell et al. 2009), lattice vibrations (Huber et al. 2008a, b), and mobile carriers (Huber et al. 2008a, b).

In this study, silica-coated gold and pure silica nanoparticles drop-casted on silicon substrate are investigated by s-SNOM. This is performed to quantify the wavelength and size dependent near-field resonant phonon polariton interactions of silica-shell/Au-core nanoparticles in a wavelength region where silica has a vibrational optical phonon resonance. By taking advantage of the thin coating layers of silica on the high index Au-core, we achieved strong near-field resonant phonon polariton interactions between the metallic probing tip and the thin silica-shell. The sensitivity of s-SNOM imaging is known to improve if the sample of interest (e.g., nanoparticles or thin films) is placed on substrates with a high refractive index (e.g., Si or Au) due to near-field coupling between the tip and substrate. Strong phase contrast is observed in capped particles with a thin silica-shell, which is comparable to pure silica particles of similar height, near the wavelength where near-field phonon resonant interaction between the silica-shell and the probing tip is expected. This is because of the enhanced near-field interaction of the probing tip with the high index Au-core in the capped particles. Substrate enhanced s-SNOM allows spectroscopic identification of nanocomposites with nanometer resolution. This capability of s-SNOM should lead to the investigation of several important problems related to self assembled monolayers, thin oxide layers, photoresists, and coatings.

Experimental setup and theoretical model

Nanoparticle samples were prepared on a Si substrate first cleaned by sonication in methanol and dried with nitrogen gas. The substrate was then dipped in a 0.1% APTMS (3-aminopropyltrimethoxysilane) solution in ethanol, rinsed with pure ethanol and dried with nitrogen gas. Nanoparticle solutions (nanoComposix, nanocomposix.com) diluted with isopropyl alcohol were drop-casted on the wafer, allowed to react for 12.5 min, then were rinsed and dried with ethanol and nitrogen gas, respectively. Figure 1 shows transmission electron-microscopy (TEM) images of monodispersed silica-shell/Au-core nanoparticles and pure silica nanoparticles used in these experiments. The TEM images shown in Fig. 1 indicate the shapes of the composite silica–Au nanoparticles and the thicknesses of the silica-shell (average size of ~ 10 nm) are highly uniform. Size statistics performed on these samples (not shown) demonstrate size distributions of 10–20%, typical values for many colloidal syntheses.

Simultaneous topography, infrared amplitude, and phase contrast imaging is performed using a commercial s-SNOM setup (NeaSNOM, neaspec.com) shown in Fig. 2 by recording the line-tunable infrared carbon dioxide laser light scattered from commercial, Pt-coated, cantilevered, Si tips. The vertical oscillation frequency of the tip is 286 kHz with amplitude of ~ 20 nm. We achieve near-field scattering measurements using a combination of demodulation of the detector signal at higher harmonics of the resonance frequency, $n\Omega$ (demodulation order $n > 1$), and a pseudoheterodyne interferometric signal detection scheme for greater background suppression (Ocelic et al. 2006). The pseudoheterodyne detection technique allows simultaneous measurement of near-field optical signal amplitude and phase by interferometric detection of scattered light using a phase-modulated reference wave. This technique has been shown to provide a reliable near-field optical material contrast with a higher background suppression efficiency and ease of implementation compared to other interferometric detection methods (Ocelic et al. 2006).

While probing nanoscale optical properties of a homogeneous flat sample surface located below the illuminated tip, the scattered light and thus the near-field optical image contrast can be explained by approximating the probe as a dipole located at the tip apex (Knoll and Keilmann 2000). The near-field

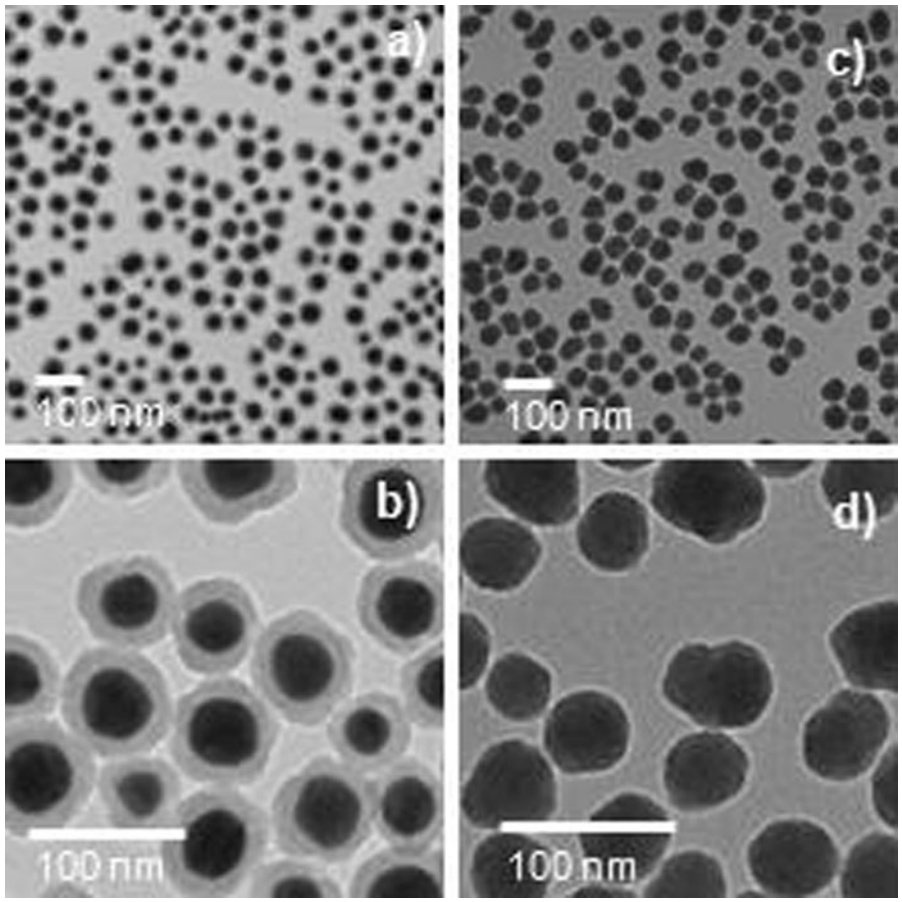

Fig. 1 Typical TEM images of monodispersed silica-shell/Au-core (**a**) and pure silica (**c**) nanoparticles used in these experiments. A closer view of TEM images of few nanoparticles (silica-shell/Au-core (**b**) and pure silica (**d**)) which shows uniform thickness of the silica capping layer covering Au nanoparticle core

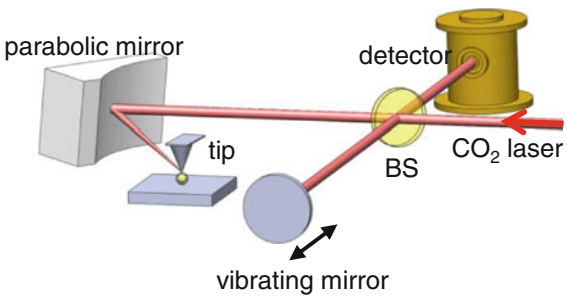

Fig. 2 Schematic of the experimental setup (NeaSNOM, neaspec.com), based on a tapping mode atomic force microscope. A Michelson interferometer is used for detecting the light scattered by the tip. BS labels the beam splitter of the interferometer

interaction between the tip dipole and its mirror image in the sample result in amplitude and phase signals of the scattered light that depend on the local dielectric function of the sample (Hillenbrand and Keilmann 2002). If the sample exhibits infrared vibrational resonances, s-SNOM optical images can be considered as the resonant near-field interactions between the sample surface and the probing tip (Stiegler et al. 2011). In SiO_2, for example, which has longitudinal optical phonon frequency in the mid IR, the characteristic near-field contrasts stem from a phonon–polariton resonant near-field interaction (which peaks starting around $\sim 1000\ cm^{-1}$) between the probing tip and the SiO_2 sample surface (Huber et al. 2010). For the thin sample coating layer of SiO_2 on a spherical Au nanoparticle core studied in our work, a similar near-field polariton interaction can be predicted by performing theoretical calculations of the amplitude and phase spectra using an extended dipole–dipole coupling model. The model is based on the solution of the electrostatic boundary-value problem (Laplace's

equation) for a system of many interacting dipoles in the presence of a substrate (Abate et al. 2009; Cvitkovic et al. 2006; Gozhenko et al. 2003). In this model, the extended structure of the probing tip is approximated by a point dipole at the extreme end of the tip. The nanoparticles are also approximated as point dipoles; both the tip dipole and the nanoparticle dipole interact with their own image dipoles generated by the sample surface. The combined polarizability is then described by the sum of the polarizability of the tip dipoles and the nanoparticle dipoles. Since the total polarizability depends on the local dielectric function of the sample, the near-field optical infrared images can thus be considered as dielectric maps of the sample surface where the spatial resolution is given by the size of the tip apex. In capped nanoparticles, the dielectric function of the hybrid core–shell nanoparticle (silica-shell/Au-core) is included in the simulation as a single dielectric function taken from Fofang et al. (2008) and Wiederrecht et al. (2004) that includes the dielectric constant of the metal core and the dielectric constant of the silica-shell. The dielectric function for the silica layer is described by a simple damped harmonic oscillator as described by Huber et al. (2010); the model is further improved by taking into account the tip vibration amplitude ($\sim$20 nm) and signal harmonic demodulation to simulate experimental conditions. The demodulated 2nd harmonic signal is numerically calculated by Fourier transforming the modulated effective polarizability.

The extended dipole model is applied here to calculate the IR s-SNOM near-field polariton interaction of silica-shell/Au-core spherical nanoparticles, in amplitude and phase, as a function of the diameter of the particles. Figure 3 shows the results obtained at $\omega = 1080\ \mathrm{cm}^{-1}$ near SiO_{2-} resonant tip-particle phonon polariton interaction is expected and at $\omega = 952\ \mathrm{cm}^{-1}$ where such interaction is not expected. We find stronger amplitudes s_2 and phase signals at $\omega = 1080\ \mathrm{cm}^{-1}$ than at $\omega = 952\ \mathrm{cm}^{-1}$. In general, for a given diameter of a particle we find an increasing amplitude and phase signals as longer wavelengths are used toward SiO_2 phonon resonance. This is due to the increasing resonant tip-particle phonon polariton interaction. Below a particle size of about 1/3 of the tip radius, the wavelength dependent signals cannot be distinguished, as the coupling between the particle and the tip becomes negligible compared to the much stronger coupling between the tip and the substrate.

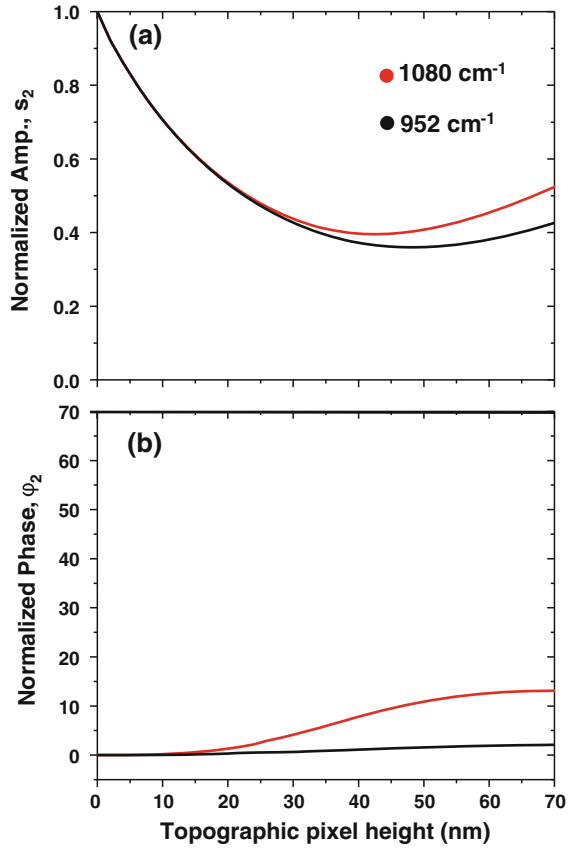

Fig. 3 Second harmonic demodulated near-field amplitude s_2 and phase φ_2 spectra obtained from extended dipole model for silica-shell/Au-core nanoparticles on a silicon substrate at two selected laser frequencies, $\omega = 1080\ \mathrm{cm}^{-1}$ (*red line*) and $\omega = 952\ \mathrm{cm}^{-1}$ (*black line*). Phase signals are plotted in units of degrees. All values are normalized to that of the Si substrate. (Color figure online)

Results and discussions

In Fig. 4 we show topography and optical images in amplitude and phase of silica capped Au nanoparticles on a silicon substrate at two of the laser frequencies, $\omega = 1080\ \mathrm{cm}^{-1}$ and $952\ \mathrm{cm}^{-1}$. In the amplitude images the particles appear darker than the substrate and in the phase images they appear brighter. At $1080\ \mathrm{cm}^{-1}$ where a phonon polariton resonance is expected a much stronger phase signal φ_2 (Fig. 4c) is observed (Brendel and Bormann 1992). The phase contrast is much weaker at off resonance ($952\ \mathrm{cm}^{-1}$) as shown in Fig. 4f.

In Fig. 5 we show experimental data points of amplitude (Fig. 5a, c) and phase (Fig. 5b, d) of pure silica and silica-shell/Au-core nanoparticles at the two

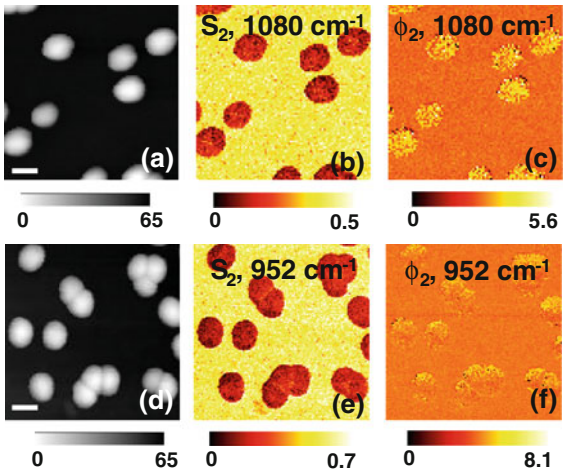

Fig. 4 Topography and near-field images of silica-shell/Au-core nanoparticles on a silicon substrate. **a**, **b** and **c** are topography, near-field amplitude and phase images, respectively, at $\omega = 1080\ \text{cm}^{-1}$, (**d**, **e** and **f** are topography, near-field amplitude and phase images, respectively, at $\omega = 952\ \text{cm}^{-1}$. The *bars* on topography all indicate 100 nm *scale*

laser frequencies, $\omega = 1080\ \text{cm}^{-1}$ and $952\ \text{cm}^{-1}$. Each experimental data point plotted in Fig. 5 represents an average signal value of pixels taken near the center of a particle. Capped and uncapped particles exhibit similar signal difference in amplitude and phase at the two wavelengths displayed. Both the amplitude and phase signals are larger at $\omega = 1080\ \text{cm}^{-1}$ than at $\omega = 952\ \text{cm}^{-1}$ in both capped and uncapped particles. The larger amplitude observed at $\omega = 1080\ \text{cm}^{-1}$ (near SiO_{2-} phonon polariton resonance) compared to that at $\omega = 952\ \text{cm}^{-1}$ is to be expected due to resonant tip-particle phonon polariton interaction. Strikingly we note the similarity in the phase signal difference at the two wavelengths for the capped and uncapped particles. In our recent work (Stiegler et al. 2011), we reported that the near-field phase spectra of small particles reveals their absorption characteristics. Since the amount of SiO_2- material in silica-shell/Au-core (with shell thickness ~ 10 nm) particle is much smaller than in a pure silica particle of the same height we expected less absorption and as a result weaker phase in the capped particle signals, contrary to what was observed.

The spectral phonon polariton signature of the silica capped and pure silica particles is measured in amplitude s_2 and phase φ_2 by taking images at 6 different frequencies (Fig. 6). Quantitative near-field amplitude and phase measurements were extracted from the raw data, by averaging the pixel values of the same area of a nanoisland surface to get topographic height values and corresponding near-field amplitude and phase signal values. Careful attention has been given to correlate average topographic, amplitude, and phase values to the same area by correcting the spatial drift between the different images at different

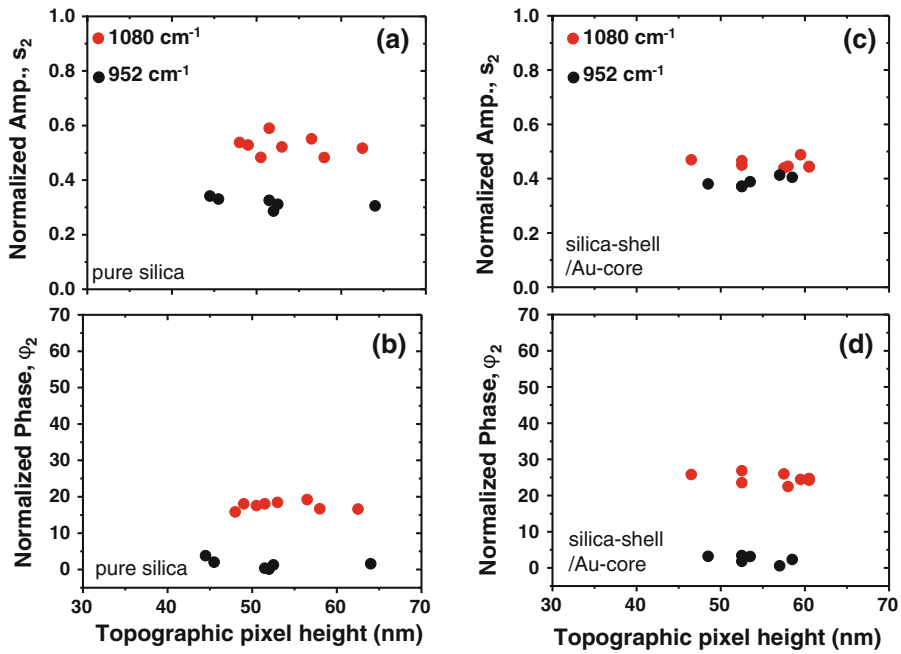

Fig. 5 Experimental amplitude data points of pure silica nanoparticles (**a**) and silica-shell/Au-core nanoparticles (**c**). Experimental phase data points of pure silica nanoparticles (**b**) and silica-shell/Au-core (**d**) at two of the laser frequencies, $\omega = 1080\ \text{cm}^{-1}$ (*red dots*) and $\omega = 952\ \text{cm}^{-1}$ (*black dots*). (Color figure online)

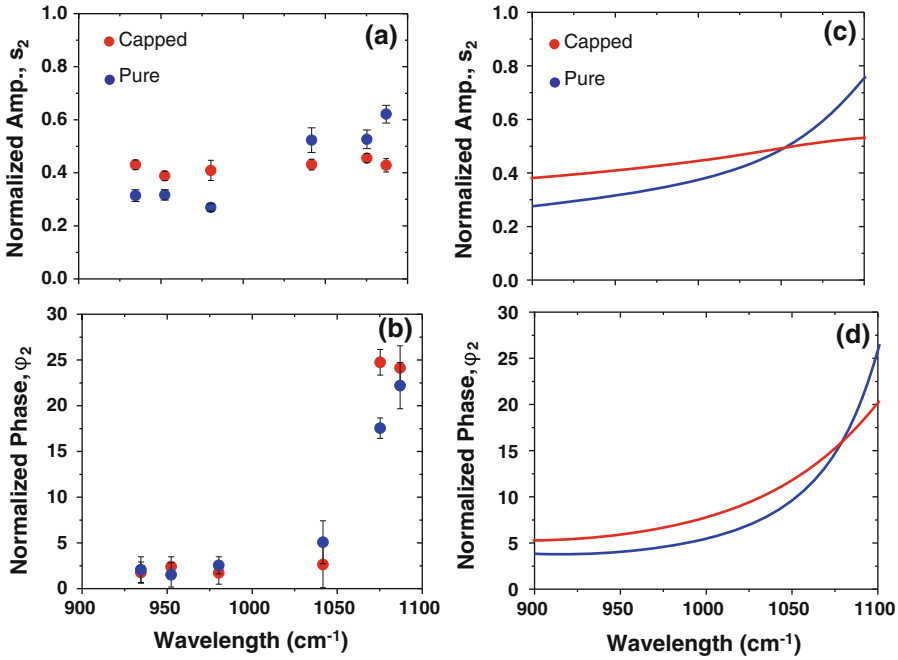

Fig. 6 Second harmonic demodulated near-field amplitude s_2 and phase φ_2 spectra obtained from s-SNOM images of silica capped-Au and pure silica nanoparticles on a silicon substrate. *Red points* and *lines* represent results for silica capped Au nanoparticles and *blue points* and *lines* represent results for silica nanoparticles, **a** experimental amplitude s_2, with *error bars* **b** experimental phase φ_2 spectra with *error bars* **c** calculated amplitudes s_2 and **d** calculated phases φ_2 spectra. Phase signals are plotted in units of degrees. All values are normalized to that of the Si substrate. (Color figure online)

wavelengths. Signals are then taken on an area on the Si surface and the average amplitude and phase values are calculated for this region at each wavelength. Near-field amplitude values were found by taking the ratio between signal values on the nanoparticles and signal values on the Si surface. The phase values were calculated in degrees by taking the difference between the signal values on the nanoparticles and Au surface at each wavelength. The phase spectra show a phonon polariton resonance that starts to peak at around 1050 cm^{-1} (Fig. 6b) for both capped and uncapped particles and the amplitude spectra shows stronger contrast at higher frequency for the pure particles than that of the capped particles (Fig. 6a).

To aid the interpretation of the experimental data, we performed theoretical calculations of the amplitude and phase spectra using the extended dipole–dipole coupling model described above. The model calculation results for the second harmonic demodulated near-field amplitudes s_2 and phase φ_2 spectra are shown in Fig. 6c, d. The calculation confirms experimental results in both the near-field amplitude s_2 and phase φ_2 spectra. The normalized near-field amplitude contrast of the capped particles is larger than that of the pure particles at off resonance frequencies (Fig. 6c). In mid IR frequencies, the amplitude contrast between Au and Si substrate is weak compared to visible frequencies. In addition, in mid IR frequencies where there phonon resonant tip-particle coupling is absent, the silica capping layer with a high index contributes significantly to the near-field scattering (Amarie and Keilmann 2011). As a result of the combined effect of the dielectric values of the Au and the capping layer, the normalized amplitude signal of a capped particle will be smaller compared to the pure silica particle at mid IR frequencies at off-phonon polariton tip-particle coupling region as can be seen in Fig. 6a, c. We note that although the average amplitude signal contrast difference between capped and uncapped particles is in general weak at mid IR, identification of particles in the amplitude image is still possible since the normalized s_2 for pure particles is ~ 0.30 and ~ 0.40 for capped particles between $\omega = 900$–1000 cm^{-1}. At near-resonance frequency the amplitude contrast of the pure particles is larger than capped particles due to

stronger phonon resonant near-field coupling in pure particles than capped particles which results in a stronger amplitude contrast.

On the other hand, both the pure silica particle and the silica-shell/Au-core particles result in a higher phase contrast at higher frequency (>1,000 cm^{-1}) as shown in Fig. 6b, d. The near-field amplitude and phase spectral characteristics of SiO_2 are well explored by Huber et al. (2010) in a similar wavelength range considered in our work. In their work, the authors have shown that the characteristic near-field contrasts of SiO_2 stem from a phonon–polariton resonant near-field interaction (which starts to peak around 1,000 cm^{-1}) between the probing tip and the SiO_2 nanostructures. Both our experimental and theoretical calculation results for pure SiO_2 particles show a similar increasing trend toward lower wavelength as reported by Huber et al. (2010). The pure silica particles and the silica-shell/Au-core particles result in a higher phase contrast at higher frequency (>1,000 cm^{-1}) where phonon resonant tip-particle interaction is expected. Due to the correlation of the near-field phase spectra with absorption spectra the strong phase contrast observed at higher frequency for the pure particles is not surprising. For capped particles however the silica-shell is only $\sim$10 nm thick and still exhibits comparable phase contrast as pure particles at higher frequencies. This is because of the strong near-field interaction of the probing tip with the high index Au-core in the capped particles. The use of a metallic substrate such as gold for infrared wavelengths enhances the spectroscopic near-field signals of a vibrational fingerprint of the thin sample layer (Aizpurura et al. 2008). This is due to the strong reflection of the incident radiation at the substrate enhances the tip illumination and the enhanced tip-substrate near-field interaction further increases the local field acting on very thin sample layers (thickness <25 nm) thereby enhancing the near-field phase signals: which is a manifestation of the absorption spectra. Although the thin silica-shell in the capped particles contains less absorbing material compared to that of a pure silica particle, the strong near-field interaction of the Au-core with the metallic tip allows the capped particles to exhibit strong phase contrast.

In conclusion, we have imaged single silica-shell/Au-core and pure silica nanoparticles in the infrared frequency range using s-SNOM. The capped particles with a thin silica-shell show strong near-field optical contrasts. These are comparable to contrasts of pure silica particles of similar diameter near the wavelength where near-field phonon resonant interactions between the silica-shell and the probing tip are expected. The observed strong optical contrasts of the capped nanoparticles are attributed to the strong near-field interaction of the Au-core and the probing tip. Experimental near-field amplitude and phase qualitative interpretations of s-SNOM images are supported by extended dipole model calculations which take into account the near-field coupling between the probe tip, the silica-shell, and the Au-core below the shell.

Acknowledgments The financial support provided by the Department of Physics and Astronomy and the College of Natural Science and Mathematics (CNSM), California State University, Long Beach (startup grant), the American Chemical Society, Petroleum Research Fund (ACS PRF) under grant PRF# 50461-UNI10 and from Research Corporation for Science Advancement Award are all gratefully acknowledged.

References

Abate Y, Schwartzberg A, Strasser D, Leone S (2009) Nanometer-scale size dependent imaging of cetyl trimethyl ammonium bromide (CTAB) capped and uncapped gold nanoparticles by apertureless near-field optical microscopy. Chem Phys Lett 474:146–152

Aizpurura J, Taubner T, Abajo F, Drehm M, Hillenbrand R (2008) Substrate-enhanced infrared near-field spectroscopy. Opt Express 16:1529–1545

Amarie S, Keilmann F (2011) Broadband-infrared assessment of phonon resonance in scattering-type near-field microscopy. Phys Rev B 83:045404

Amarie S, Ganz T, Keilmann F (2009) Mid-infrared near-field spectroscopy. Opt Express 17:21794–21801

Bao A, Lai H, Yang Y, Liu Z, Tao C, Yang H (2010) Luminescent properties of YVO_4:Eu/SiO_2 core–shell composite particles. J Nanopart Res 12:635–643

Basiruddin S, Saha A, Pradhan N, Jana N (2010) Advances in coating chemistry in deriving soluble functional nanoparticle. J Phys Chem C 114:11009–11017

Berndt I, Pedersen J, Richtering W (2006) Temperature-sensitive core–shell microgel particles with dense shell. Angew Chem Int Ed 45:1737–1741

Brendel R, Bormann D (1992) An infrared dielectric function model for amorphous solids. J Appl Phys 71:1–6

Cvitkovic A, Ocelic N, Aizpurua J, Guckenberger R, Hillenbrand R (2006) Infrared imaging of single nanoparticles via strong field enhancement in a scanning nanogap. Phys Rev Lett 97:060801

Fofang N, Park T, Neumann O, Mirin N, Nordlander P, Halas N (2008) Plexcitonic nanoparticles: plasmon-exciton coupling in nanoshell−j-aggregate complexes. Nano Lett 8:3481–3487

Gozhenko V, Grechko L, Whites K (2003) Electrodynamics of spatial clusters of spheres: substrate effects. Phys Rev B 68:125422

Hillenbrand R, Keilmann F (2002) Material-specific mapping of metal/semiconductor/dielectric nanosystems at 10 nm resolution by backscattering near-field optical microscopy. Appl Phys Lett 80:25–27

Hu X, Gao X (2010) Silica–polymer dual layer-encapsulated quantum dots with remarkable stability. ACS Nano 4: 6080–6086

Huber A, Ocelic N, Taubner T, Hillenbrand R (2006) Nanoscale resolved infrared probing of crystal structure and of plasmon-phonon coupling. Nano Lett 6:774–778

Huber A, Deutsch B, Novotny L, Hillenbrand R (2008a) Focusing of surface phonon polaritons. Appl Phys Lett 92:203104

Huber A, Keilmann F, Wittborn J, Aizpurua J, Hillenbrand R (2008b) Terahertz near-field nanoscopy of mobile carriers in single semiconductor nanodevices. Nano Lett 8:3766–3770

Huber A, Wittborn J, Hillenbrand R (2010) Infrared spectroscopic near-field mapping of single nanotransistors. Nanotechnology 21:235702

Kim Z, Leone S (2006) High-resolution apertureless near-field optical imaging using gold nanosphere probes. J Phys Chem B 110:19804–19809

Kim D, Heo J, Ahn S, Han S, Yun W, Kim Z (2009) Real-space mapping of the strongly coupled plasmons of nanoparticle dimers. Nano Lett 9:3619–3625

Knoll B, Keilmann F (2000) Enhanced dielectric contrast in scattering-type scanning near-field optical microscopy. Opt Commun 182:321–328

Lawrie G, Battersby B, Trau M (2003) Synthesis of optically complex core–shell colloidal suspensions: pathways to multiplexed biological screening. Adv Funct Mater 13:887–896

Ocelic N, Huber A, Hillenbrand R (2006) Pseudoheterodyne detection for background-free near- field spectroscopy. Appl Phys Lett 89:101124

Ogawa Y, Minami F, Abate Y, Leone S (2010) Nanometer-scale dielectric constant of Ge quantum dots using apertureless near-field scanning optical microscopy. Appl Phys Lett 96:063107

Schnell M, Garcia-Etxarri A, Huber A, Crozier K, Aizpurua J, Hillenbrand R (2009) Controlling the near-field oscillations of loaded plasmonic nanoantennas. Nature Photon 3:287–297

Stiegler J, Abate Y, Cvitkovic A, Romanyuk Y, Huber A, Leone S, Hillenbrand R (2011) Nanoscale infrared absorption spectroscopy of individual nanoparticles enabled by scattering-type near-field microscopy. ACS Nano 5:6494–6499

Teng F, Tian Z, Xiong G, Xu Z (2004) Preparation of CdS–SiO_2 core-shell particles and hollow SiO_2 spheres ranging from nanometers to microns in the nonionic reverse microemulsions. Catal Today 93:651–656

Wang Y, Dave R, Pfeffer R (2004) Polymer coating/encapsulation of nanoparticles using a supercritical anti-solvent process. J Supercrit Fluids 28:85–99

Wiederrecht G, Wurtz G, Hranisavljevic J (2004) Coherent coupling of molecular excitons to electronic polarizations of noble metal nanoparticles. Nano Lett 4:2121–2125

Yu M, Lin J, Fang J (2005) Silica spheres coated with YVO_4:EU^{3+} layers via sol−gel process: a simple method to obtain spherical core−shell phosphors. Chem Mat 17: 1783–1791

Zimmer J, Kim S, Ohnishi S, Tanaka E, Frangioni J, Bawendi M (2006) Size series of small indium arsenide-zinc selenide core-shell nanocrystals and their application to in vivo imaging. J Am Chem Soc 128:2526–2527

Zou B, Little R, Wang J, Sayed-El M (1999) Effect of different capping environments on the optical properties of CdS nanoparticles in reverse micelles. Int J Quant Chem 72: 439–450